JOURNAL OF NEUROTRAUMA 28:649–660 (April 2011)

DOI: 10.1089/neu.2010.1662

Consistent Injury to Medium Spiny Neurons and White Matter in the Mouse Striatum after Prolonged Transient Global Cerebral Ischemia

Hideyuki Yoshioka, Kuniyasu Niizuma, Masataka Katsu, Hiroyuki Sakata, Nobuya Okami, and Pak H. Chan

Abstract

A reproducible transient global cerebral ischemia (tGCI) mouse model has not been fully established. Although striatal neurons and white matter are recognized to be vulnerable to ischemia, their injury after tGCI in mice has not been elucidated. The purpose of this study was to evaluate injuries to striatal neurons and white matter after tGCI in C57BL/6 mice, and to develop a reproducible tGCI model. Male C57BL/6 mice were subjected to tGCI by bilateral common carotid artery occlusion (BCCAO). Mice whose cortical cerebral blood flow after BCCAO decreased to less than 13% of the pre-ischemic value were used. Histological analysis showed that at 3 days after 22 min of BCCAO, striatal neurons were injured more consistently than those in other brain regions. Quantitative analysis of cytochrome c release into the cytosol and DNA fragmentation in the striatum showed consistent injury to the striatum. Immunohistochemistry and Western blot analysis revealed that DARPP-32-positive medium spiny neurons, the majority of striatal neurons, were the most vulnerable among the striatal neuronal subpopulations. The striatum (especially medium spiny neurons) was susceptible to oxidative stress after tGCI, which is probably one of the mechanisms of vulnerability. SMI-32 immunostaining showed that white matter in the striatum was also consistently injured 3 days after 22 min of BCCAO. We thus suggest that this is a tGCI model using C57BL/6 mice that consistently produces neuronal and white matter injury in the striatum by a simple technique. This model can be highly applicable for elucidating molecular mechanisms in the brain after global ischemia.

Key words: global cerebral ischemia; medium spiny neurons; mice; striatum; white matter

Introduction

A brief period of transient global cerebral ischemia (tGCI; i.e., 5–10 min) induces delayed neuronal cell death mainly in the hippocampal CA1 subregion in rats and gerbils (Kirino, 1982; Pulsinelli et al., 1982). Many trials have been attempted in mice to establish a tGCI model that produces consistent CA1 injury, with only modest success (Fujii et al., 1997; Murakami et al., 1998; Olsson et al., 2003; Panahian et al., 1996; Sheng et al., 1999; Wellons et al., 2000; Yang et al., 1997; Yonekura et al., 2004).

Besides the CA1 subregion, the striatum is also recognized to be vulnerable to ischemia. The striatum is the largest nucleus of the basal ganglia, and dysfunction of the striatum has been associated with neurodegenerative disorders such as Huntington's disease. Anatomically, striatal neurons fall into two main classes: spiny projection neurons and aspiny interneurons. Spiny projection neurons, also known as medium spiny neurons (MSNs), make up approximately 95% of the striatal neurons. Aspiny interneurons, the remaining 5%, can be categorized into medium GABAergic interneurons and large cholinergic interneurons (Kreitzer, 2009). Although MSNs are reported to be the most vulnerable to tGCI of the striatal neurons (Terashima et al., 1998; Yoshioka et al., 2010), quantitative evaluation of their vulnerability has not been studied.

In contrast, injury to white matter, which is composed of myelinated axons and oligodendrocytes, has been the focus of much attention in cerebral ischemia research in recent years. White matter injury has also been observed in patients who suffer from transient cardiac arrest, and the prognosis has been reported to be worse in patients with severe white matter injury (Wu et al., 2009). Understanding the mechanism of white matter injury using an animal model is necessary for

Department of Neurosurgery, Department of Neurology and Neurological Sciences, and Program in Neurosciences, Stanford University School of Medicine, Stanford, California.

development of new treatments. However, white matter injury after tGCI, which mimics conditions after cardiac arrest, has not been elucidated.

Since C57BL/6 mice are commonly used in the production of transgenic animals (Keskintepe et al., 2007), development of a tGCI model in this strain is extremely important to clarify the mechanisms of injury. The purpose of this study was to evaluate injuries to the striatum and white matter after tGCI in C57BL/6 mice, and to develop a reproducible tGCI model. We found that striatal neurons, especially MSNs, were the most consistently injured in the mouse brain after relatively prolonged global ischemia. Furthermore, we observed that striatal white matter, through which the fiber fascicles of the internal capsule run in rodents, was consistently injured after tGCI. Here we propose a striatal tGCI model, using C57BL/6 mice, that induces consistent injury to neurons and white matter.

Methods

Global cerebral ischemia

All animals were treated in accordance with Stanford University guidelines, and the animal protocols were approved by Stanford University's Administrative Panel on Laboratory Animal Care. Male C57BL/6J mice (8–12 weeks old; The Jackson Laboratory, Bar Harbor, ME) were used. Anesthesia was induced with inhalation of 4% isoflurane and intraperitoneal injection of xylazine (4 mg/kg), and maintained with 1.5% isoflurane in 70% nitrous oxide and 30% oxygen via facemask. Rectal temperatures were maintained at 37 ± 0.5°C with a heating blanket (Harvard Apparatus, Holliston, MA) and a heating lamp. An anterior midline incision was made in the neck, and both common carotid arteries were exposed and loosely encircled with 3-0 silk to enable later occlusion. Regional cerebral blood flow (rCBF) was monitored by laser Doppler flowmetry (LDF) (Laserflo BMP^2; Vasamedics, Eden Prairie, MN). The probe was fixed on the skull 4 mm lateral to the bregma. Changes in rCBF after bilateral common carotid artery occlusion (BCCAO) were expressed as a percentage of the pre-ischemic value. BCCAO was induced by applying microaneurysm clips (Roboz, Gaithersburg, MD) to both common carotid arteries for a period of 10, 15, 22, or 30 min. Immediately after occlusion, anesthesia was turned off. To reperfuse, the animals were briefly re-anesthetized with 1% isoflurane, and the clips were removed. After observing blood flow return, the skin incision was sutured and the animals were wrapped with a heating blanket to maintain rectal temperatures above 36.0°C for 24 h after surgery. Acetated Ringer's solution (0.5 mL) was administered subcutaneously to all animals 30 min and 24 h after ischemia.

In a separate group of mice subjected to 22 min of BCCAO, blood pressure was measured through a PE-10 cannula inserted into the left femoral artery. Arterial blood samples were analyzed with a blood gas analyzer (i-STAT; Abbott Laboratories, Abbott Park, IL).

Carbon black evaluation of patency of the posterior communicating arteries

We evaluated the relationship between rCBF after 1 min of BCCAO and patency of the posterior communicating artery (PcomA) as a preliminary experiment ($n = 10$). Carbon black ink was injected as described previously (Murakami et al., 1998). Patency of the PcomA was assessed by comparing its diameter on each side with the diameter of the basilar artery, and grading it as 0 or 1 (grade 0, PcomA diameter $< 1/3$ of basilar artery diameter; grade 1, PcomA diameter $\geq 1/3$ of basilar artery diameter). Thus the sum of the scores from both sides was 0, 1, or 2 (Kitagawa et al., 1998).

Histological analysis of ischemic neuronal injury

For histological analysis, the mice were subjected to 10 ($n = 15$), 15 ($n = 18$), 22 ($n = 25$), or 30 ($n = 27$) min of BCCAO. Three days after ischemia, the brains were removed and sectioned at 30 μm with a vibratome. Brain sections 0.5 mm anterior (striatum) and 2.0 mm posterior (hippocampus, cerebral cortex, and thalamus) to the bregma were stained with cresyl violet. A blinded investigator assessed ischemic injury using a grading scale (0 = no damage; 1 = 1–20%; 2 = 21–40%; 3 = 41–60%; 4 = 61–80%; 5 = 81–100%), and each hemisphere was examined independently.

Immunohistochemistry

Anesthetized animals were perfused with 10 U/mL heparin saline and subsequently with 4% paraformaldehyde in phosphate-buffered saline 6, 24, or 72 h or 7 days after 22 min of BCCAO. The brains were removed, post-fixed for 24 h, and cut on a vibratome into slices 30 μm thick. For diaminobenzidine immunohistochemistry, the avidin-biotin technique was used. Nuclei were counterstained with hematoxylin solution.

Double-immunostaining was performed with immunofluorescence. Brain sections were reacted with primary antibodies, then incubated with appropriate Alexa Fluor 488- and 594-conjugated immunoglobulin G antibodies (Invitrogen, Carlsbad, CA). Negative controls were treated with similar procedures, except that the primary antibody was omitted. The sections were covered with VECTASHIELD mounting medium with 4',6-diamidino-2-phenylindole (DAPI; Vector Laboratories, Burlingame, CA), and examined under an LSM510 confocal laser scanning microscope or an Axioplan 2 microscope (Carl Zeiss, Thornwood, NY).

We used the following as primary antibodies: anti-dopamine and cyclic AMP-regulated phosphoprotein of relative molecular weight 32,000 (DARPP-32, as an MSN marker; 1:400, #2306; Cell Signaling Technology, Beverly, MA), anti-choline acetyltransferase (ChAT) (as a cholinergic interneuron marker; 1:200, #AB143; Millipore, Billerica, MA), anti-somatostatin (SST, as a GABAergic interneuron marker; 1:100, #AB5494; Millipore), anti-glial fibrillary acidic protein (GFAP, as an astrocyte marker; 1:500, #AB5804; Millipore), anti-ionized calcium-binding adaptor molecule 1 (Iba-1, as a microglia marker; 1:500, #019-19741; Wako Pure Chemical Industries, Osaka, Japan), anti-8-oxoguanine (8-oxoG, 1:100, #MAB3560; Millipore), anti-RIP (1:250, #MAB1580; Millipore), anti-myelin basic protein (MBP, 1:200, #ab40390; Abcam, Cambridge, MA), and anti-non-phosphorylated neurofilament (SMI-32, 1:1000, #SMI-32R; Covance, Emeryville, CA). For mouse monoclonal antibodies, the protocol provided in the M.O.M. immunodetection kit (#BMK-2202; Vector Laboratories) was followed.

For counting immunopositive cells as striatal markers, five subregions were assigned (central, dorsomedial, dorsolateral,

ventromedial, and ventrolateral), each consisting of a rectangle 430 × 341 μm in size. Immunopositive cells in each subregion on both sides of the striatum were counted by a blinded counter.

TUNEL staining

DNA fragmentation was detected by terminal deoxynucleotidyl transferase-mediated uridine 5′-triphosphate-biotin nick-end labeling (TUNEL) using a commercial kit (#11684817910; Applied Science, Indianapolis, IN). Brain sections were evaluated 6, 24, and 72 h, and 7 days after 22 min of BCCAO, according to the manufacturer's protocol. For quantification of TUNEL staining in the striatum, TUNEL-positive cells in the five subregions on both sides of the striatum were counted as described for immunohistochemistry.

Double-staining with a cellular marker was performed to identify TUNEL-positive cells in the striatum. Brain samples 24 h after BCCAO were used. After TUNEL reaction, the sections were immunostained with an anti-neuron-specific nuclear protein (NeuN) antibody (as a neuronal marker, 1:200; Millipore), anti-GFAP, or anti-Iba-1 antibody, followed by the appropriate Alexa Fluor 594-conjugated immunoglobulin G antibodies.

Western blot analysis

Both sides of the striatum were removed 6, 24, or 72 h after 22 min of BCCAO. Protein extraction of the cytosolic fractions was performed with a multiple centrifugation method as previously described (Fujimura et al., 1998). Equal amounts of cytosolic fraction samples were loaded per lane. Sodium dodecyl sulfate-polyacrylamide gel electrophoresis was performed on a 10% NuPAGE Bis-Tris gel (Invitrogen) and then immunoblotted. Anti-cytochrome c (1:1000, #556433; BD Biosciences, San Jose, CA), anti-DARPP-32 (1:400, #2306; Cell Signaling Technology), anti-ChAT (1:200, #AB144P; Millipore), or anti-SST (1:1000, #ab53165; Abcam) primary antibodies were used. After incubation with an appropriate horseradish peroxidase-conjugated secondary antibody (Cell Signaling Technology), the bound antibodies were detected by a chemiluminescence system (Pierce, Rockford, IL). β-Actin (1:100,000; Sigma-Aldrich, St. Louis, MO) was used as an internal control. Cytochrome oxidase subunit IV (1:5000; Invitrogen) was used to ensure proper fractionation. Images were scanned and the results were quantified using Multi-Analyst software (Bio-Rad Laboratories, Hercules, CA).

Cell death assay

For quantitative analysis of apoptosis-related DNA fragmentation, we used a commercial enzyme immunoassay (#11774425001; Applied Science). Both sides of the striatum were removed 72 h after 22 min of BCCAO. Protein extraction of the cytosolic fractions was prepared as described for the Western blotting method. A cytosolic volume containing 20 μg of protein was used for the enzyme-linked immunosorbent assay, according to the manufacturer's protocol.

Detection of oxidative protein damage

Both sides of the striatum were removed 24 h after 22 min of BCCAO. Tissues were homogenized and sonicated in ice-cold lysis buffer (Cell Signaling Technology) with 1% protease inhibitor mixture (Sigma-Aldrich). The homogenate was centrifuged (900*g* for 10 min at 4°C), and the resulting supernatant was used for quantification. With the use of a commercial kit (#S7150; Millipore), we observed the carbonyl groups as indicators of oxidative protein damage (Conlon et al., 2003). The samples were incubated with 2,4-dinitrophenylhydrazone (DNP), and the DNP-derivatized carbonyl groups were specifically detected by Western blotting with an anti-DNP antibody. The images were scanned and quantified as described for the Western blot analysis.

Statistical analysis

Comparisons among multiple groups were performed with analysis of variance (ANOVA), followed by a Scheffé *post-hoc* analysis (SigmaStat; Systat Software Inc., Chicago, IL). Comparisons between two groups were achieved with a Student's unpaired *t*-test. Data are expressed as mean ± standard deviation (SD), and significance was set at $p < 0.05$.

Results

Relationship between patency of the PcomA and rCBF

In 8 of 10 mice, rCBF after 1 min of BCCAO was reduced to less than 13% of the pre-ischemic value, and no patent PcomA was identified in these mice. In contrast, patent PcomAs were observed in two mice whose rCBF was not reduced to 13%. According to these results, we used only animals whose rCBF decreased to <13% of the pre-ischemic value in further studies, to exclude the variances in collateral flow through the PcomA. With this criterion, the number of excluded animals was 3/15 (20.0%), 4/18 (22.2%), 7/38 (18.4%), and 5/27 (18.5%) mice, in the 10-, 15-, 22-, and 30-min groups, respectively.

Neurological findings and mortality rate

Seizures were not observed in the 10- and 15-min groups, but were observed in 5.3% (2/38) and 18.5% (5/27) of the 22- and 30-min groups, respectively. Severe akinesia was seen 3 days after BCCAO in 0%, 8.3% (1/12), 53.3% (8/15), and 50% (4/8), of the 10-, 15-, 22-, and 30-min groups, respectively. Hyperactivity was observed in 1 mouse in the 22-min group, and hemiparesis was observed in 1 mouse in the 30-min group. The mortality rate 3 days after BCCAO was 0% (0/15), 11.1% (2/18), 18.4% (7/38), and 51.9% (14/27), in the 10-, 15-, 22-, and 30-min groups, respectively.

Physiological parameters

Physiological parameters measured in the 22-min group are listed in Table 1. Mean arterial blood pressure rose soon after BCCAO and dropped suddenly after reperfusion. rCBF was rapidly reduced after BCCAO, and remained constantly low during the ischemic period. Rectal temperature was strictly controlled during surgery, and 24 h after BCCAO it was 36.5 ± 0.4°C.

Histological analysis of ischemic injuries

Histological injury was assessed 3 days after BCCAO in the striatum, the hippocampus, the cerebral cortex, and the thalamus. There were no apparent histological injuries in the

Table 1. Physiological Parameters

	MABP (mm Hg)	*pH*	*$PaCO_2$ (mm Hg)*	*PaO_2 (mm Hg)*	*rCBF (%)*
Pre-ischemia	61.0 ± 2.2	7.31 ± 0.01	36.1 ± 3.7	146.3 ± 9.0	100
Ischemia (10 min)	80.5 ± 24.6	7.32 ± 0.01	36.1 ± 0.9	149.0 ± 9.2	6.8 ± 3.4
Post-ischemia	63.0 ± 14.8	7.28 ± 0.02	42.7 ± 5.6	163.3 ± 13.0	97.8 ± 25.1

MABP, mean arterial blood pressure; $PaCO_2$, partial arterial carbon dioxide pressure; PaO_2, partial arterial oxygen pressure; rCBF, regional cerebral blood flow.

10-min group (data not shown). In the 15-min group, many of the injuries were mild, and only a few mice showed severe injuries (Fig. 1A).

Injuries in the 22-min group were much more severe than those in the 15-min group (Fig. 1B). Severe and consistent injuries were observed in the striatum; the cells, especially small and medium-sized cells, were diffusely shrunken (Fig. 2). The striatum was uniformly injured, and there were no significant differences in severity among the five subregions (central, dorsomedial, dorsolateral, ventromedial, and ventrolateral). Severe ischemic changes (scattered and shrunken cells) were also observed in the CA1 subregion; however, these injuries were not as consistent as those in the striatum. In some mice the injuries were unilateral, and in some only the CA2–3 or CA4 subregion was injured, although the CA1 subregion was nearly intact. Bilateral ischemic injuries to the CA1 subregion were observed in 40% (6/15), and minimal to no injuries were observed in 33.3% (5/15; Fig. 1D). On the contrary, bilateral injuries to the striatum were observed in 80% (12/15), and only one mouse (6.7%) showed no injury. Injuries were also observed in the CA2, CA3, and CA4 subregions, the dentate gyrus, the cerebral cortex (mainly the second to forth layers), and the ventrolateral part of the thalamus, but these injuries were neither severe nor consistent.

The severity of injury in the 30-min group was similar to that in the 22-min group (Fig. 1C); however, we thought the ischemic duration of 30 min was not appropriate because of the high mortality rate. According to these results, we adopted the 22-min BCCAO model for further studies.

Cytochrome c release into the cytosol and cell death assay

To quantitatively confirm consistent injury to the striatum, we evaluated cytochrome c release into the cytosol using Western blot analysis, which indicates activation of the mitochondrial apoptotic pathway. In the striatum, cytochrome c in the cytosolic fraction was significantly increased 24 h after BCCAO ($p < 0.05$; Fig. 3A).

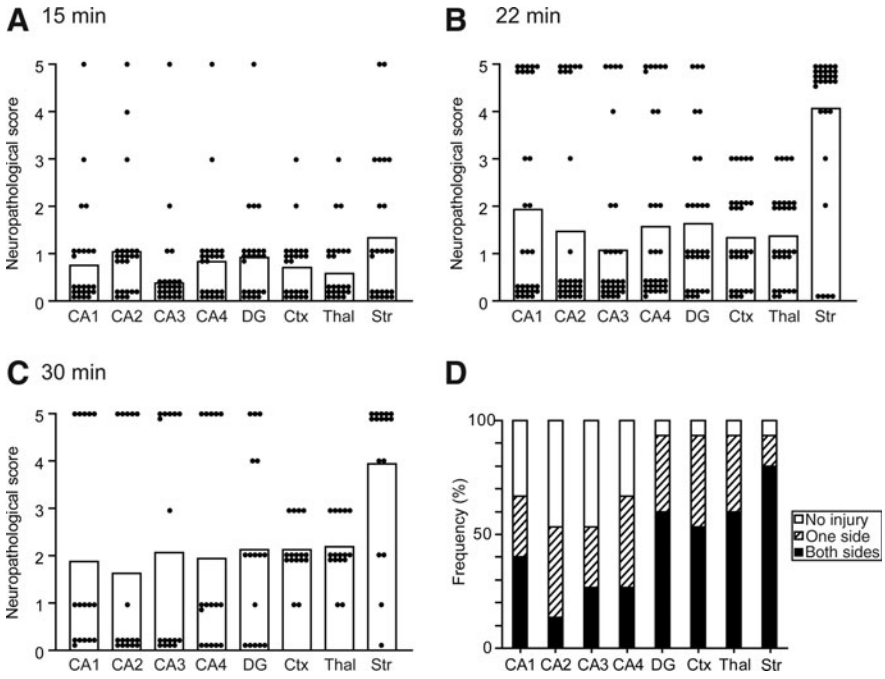

FIG. 1. (**A–C**) Neuropathological scores of the brain regions after bilateral common carotid artery occlusion (BCCAO). The individual scores are plotted as dots and the mean values are presented as columns. Ischemic injuries in the 22-min group (**B**) were much more severe compared with those in the 15-min group (**A**). Consistent injury was observed, especially in the striatum. The severity of the injury in the 30-min group (**C**) was similar to that seen in the 22-min group. (**D**) Frequency of ischemic injury in the brain regions. Bilateral injury to the striatum was observed in 80%, while injury to the CA1 subregion was seen in 40% (DG, dentate gyrus; Ctx, cortex; Thal, thalamus; Str, striatum).

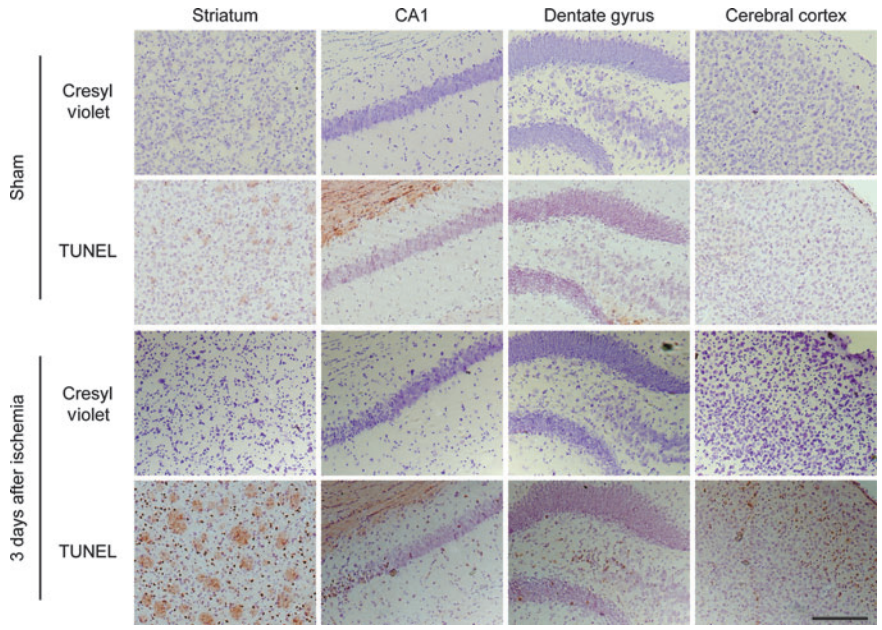

FIG. 2. Representative photomicrographs of cresyl violet and TUNEL staining in the striatum, the hippocampal CA1 subregion, the dentate gyrus, and the cerebral cortex. Three days after bilateral common carotid artery occlusion (BCCAO), the cells were diffusely shrunken in the striatum and were TUNEL-positive. Mild morphological ischemic changes in the hippocampal CA1 subregion, the CA4 subregion, the dentate gyrus, and cerebral cortex (mainly in the second to forth layers) were also observed (magnification × 100; scale bar = 200 μm; TUNEL, terminal deoxynucleotidyl transferase-mediated uridine 5′-triphosphate-biotin nick-end labeling). Color image is available online at www.liebertpub.com/neu.

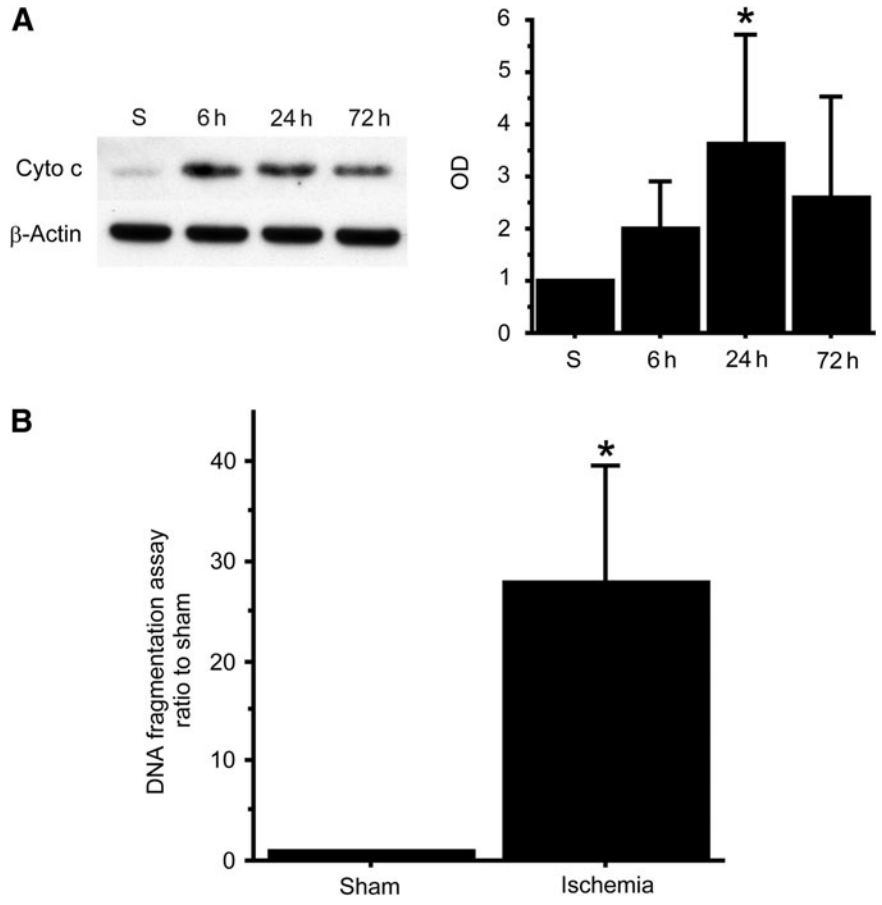

FIG. 3. (**A**) Western blot analysis shows that cytochrome c (Cyto c) in the cytosolic fraction was significantly increased in the striatum 24 h after bilateral common carotid artery occlusion (BCCAO; $n = 6$, $^*p < 0.05$). β-Actin is shown as an internal control (S, sham control; OD, optical density). (**B**) DNA fragmentation 72 h after BCCAO in the striatum was significantly increased compared with the sham animals ($n = 5$, $^*p < 0.05$).

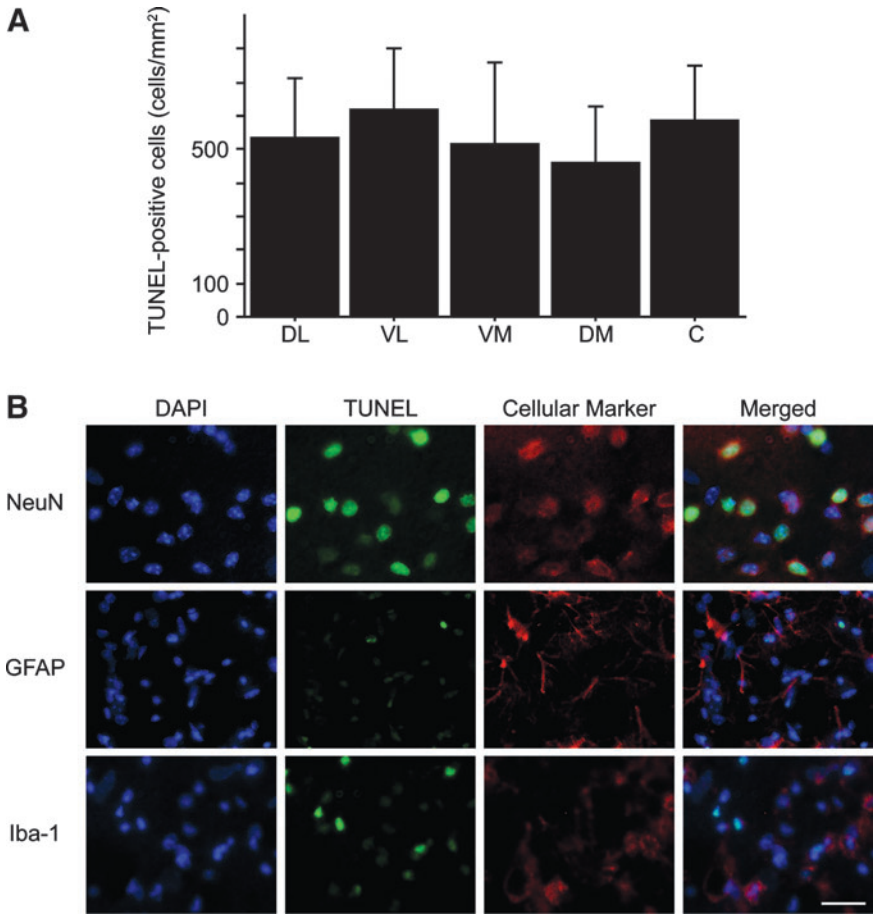

FIG. 4. (**A**) Comparison of the TUNEL-positive cells among the striatal subregions. There were no significant differences in the numbers of TUNEL-positive cells among the five subregions in the striatum ($n = 10$; DL, dorsolateral; VL, ventrolateral; VM, ventromedial; DM, dorsomedial; C, central). (**B**) Double staining showed that most of the TUNEL-positive cells (green) co-localized with NeuN (neuronal marker, red); however, they did not co-localize with GFAP (astrocyte marker), or Iba-1 (microglia marker, red). Nuclei were counterstained with DAPI (blue; magnification × 400; scale bar = 20 μm; TUNEL, terminal deoxynucleotidyl transferase-mediated uridine 5′-triphosphate-biotin nick-end labeling; NeuN, anti-neuron-specific nuclear protein; GFAP, anti-glial fibrillary acidic protein; DAPI, 4′,6-diamidino-2-phenylindole; Iba-1, anti-ionized calcium-binding adaptor molecule 1). Color image is available online at www.liebertpub.com/neu.

We also performed an apoptotic DNA fragmentation assay to quantitatively evaluate apoptosis after BCCAO. DNA fragmentation was significantly increased in the striatum compared with sham animals 72 h after BCCAO ($p < 0.05$; Fig. 3B). These results confirm that the striatum was consistently injured after 22 min of BCCAO.

TUNEL staining

TUNEL staining confirmed uniform injury to the striatum. There were no significant differences in the number of TUNEL-positive cells among the five subregions of the striatum (Fig. 4A). To identify the type of TUNEL-positive cells, we performed double staining with cellular markers. Most of the TUNEL-positive cells co-localized with NeuN; however, they did not co-localize with GFAP or Iba-1 (Fig. 4B).

Time course of striatal neuronal markers

Immunohistochemistry of the striatal neuronal markers showed the difference in ischemic vulnerability among the neuronal subpopulations. A cell counting study showed that the majority of the striatal neurons were DARPP-32-positive MSNs. In the sham animals, the numbers of DARPP-32-, ChAT-, and SST-positive cells were $1298.0 \pm 87.4/mm^2$, $26.2 \pm 10.0/mm^2$, and $28.2 \pm 5.9/mm^2$, respectively. The number of DARPP-32-positive cells significantly decreased 24–72 h after BCCAO (Fig. 5A and B); however, the number of ChAT-positive cells (cholinergic interneurons), and SST-positive cells (GABAergic interneurons) did not change after BCCAO.

Next, we quantitatively confirmed the difference in ischemic vulnerability using Western blot analysis. DARPP-32 expression significantly decreased 24–72 h after BCCAO, although there were no significant changes at any time point in ChAT and SST expression (Fig. 6). These results showed that DARPP-32-positive MSNs, the majority of striatal neurons, are the most vulnerable to tGCI of the striatal neurons.

Oxidative injury

To evaluate oxidative injury after BCCAO, we detected the carbonyl groups, which are introduced into proteins by oxidative injury (Kamada et al., 2007). In the striatum, the level of

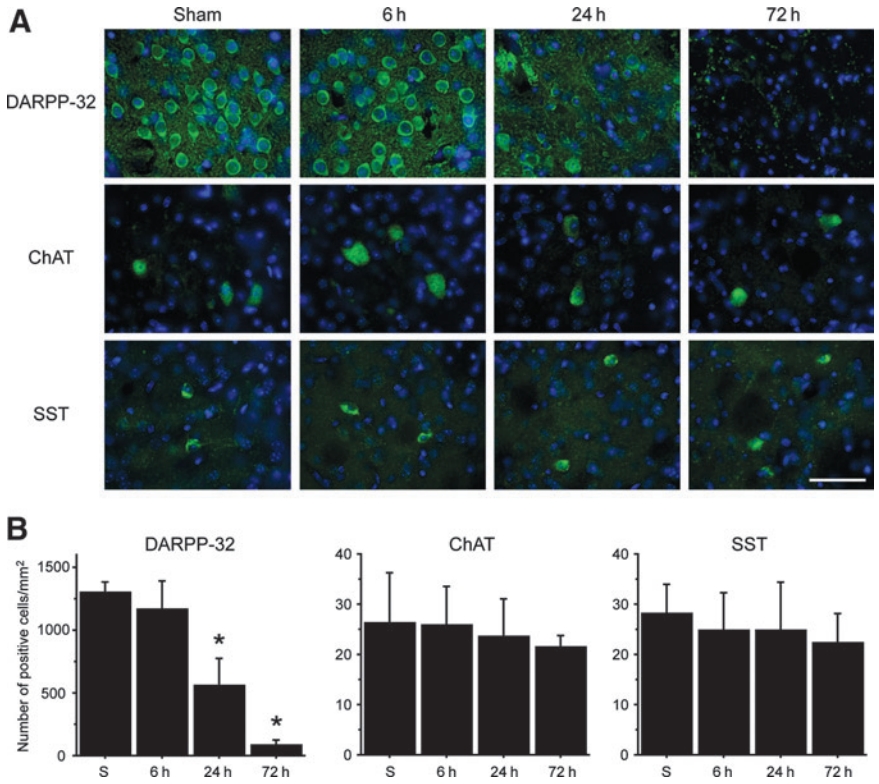

FIG. 5. (**A**) Representative photomicrographs of striatal neuronal marker staining (green). Nuclei were counterstained with DAPI (blue; magnification × 400; scale bar = 50 μm; DAPI, 4′,6-diamidino-2-phenylindole). (**B**) The cell counting study shows that the number of DARPP-32-positive cells significantly decreased 24–72 h after bilateral common carotid artery occlusion (BCCAO) compared with sham animals ($n = 4$; $^*p < 0.01$; DARPP-32, anti-dopamine and cyclic AMP-regulated phosphoprotein of relative molecular weight 32,000). However, the number of ChAT-positive cells and SST-positive cells did not change after BCCAO (S, sham control; ChAT, anti-choline acetyltransferase; SST, anti-somatostatin). Color image is available online at www.liebertpub.com/neu.

carbonyl groups 24 h after BCCAO was increased significantly compared with sham animals ($p < 0.05$; Fig. 7A and B).

DNA oxidative injury was assessed by immunohistochemical staining using an 8-oxoG antibody (Conlon et al., 2003). Expression of 8-oxoG, an oxidative product of guanine, increased in the striatum 24 h after BCCAO. 8-oxoG staining co-localized with DARPP-32 staining; however, it did not co-localize with ChAT (Fig. 7C and D) or SST staining (data not shown). These results indicate that the striatum (especially MSNs) is exceedingly susceptible to oxidative injury, which might cause the ischemic vulnerability of the striatum.

White matter injury

We evaluated white matter ischemic injury after BCCAO using immunohistochemistry. RIP immunostaining was used to detect oligodendrocytes (Hwang et al., 2006). In the sham animals, RIP immunoreactivity was observed in cell bodies and processes, which were thin and smooth. Twenty-four hours after BCCAO, the shapes of RIP-positive processes began to change, and they were tangled and intermittent 3 days after BCCAO. Seven days after BCCAO RIP-positive processes disappeared, though the staining of cell bodies was observed (Fig. 8A).

Immunostaining for neurofilament protein (SMI-32) and MBP was used to identify axonal and myelin injury, respectively. Up to 24 h after BCCAO, no obvious changes in staining were seen. At 72 h after BCCAO, there were many neuronal fibers that intensely expressed SMI-32 in the fiber fascicles of the internal capsule of the striatum. At the same time point, MBP staining of the fiber fascicles became coarse, and vacuolation of the fascicles was observed (Fig. 8B). There was no difference in the sensitivity of detection of ischemic fibers between SMI-32 and MBP staining. Using a confocal microscope, fine neurofilaments and axons could be seen in the spaces among the fiber fascicles of the striatum in the sham animals; however, they disappeared 72 h after BCCAO (Fig. 8C). Intense SMI-32 staining was also observed in the cingulum bundle, adjacent to the corpus callosum, after BCCAO (Fig. 8B). There were mild changes in the external capsule and the corpus callosum. Injury to the anterior commissure and the optic tract was not evident.

Discussion

In this study, we present a tGCI model with striatal and white matter injury in C57BL/6 mice. MSNs, the majority of striatal neurons, were consistently injured after 22 min of BCCAO. Furthermore, this model also showed consistent white matter injury in the striatum and the cingulum bundle.

Our histological evaluation showed that the striatum was injured most consistently in the brain after BCCAO. Bilateral injuries to the striatum were in particular more frequent than those to the hippocampal CA1 subregion, another vulnerable

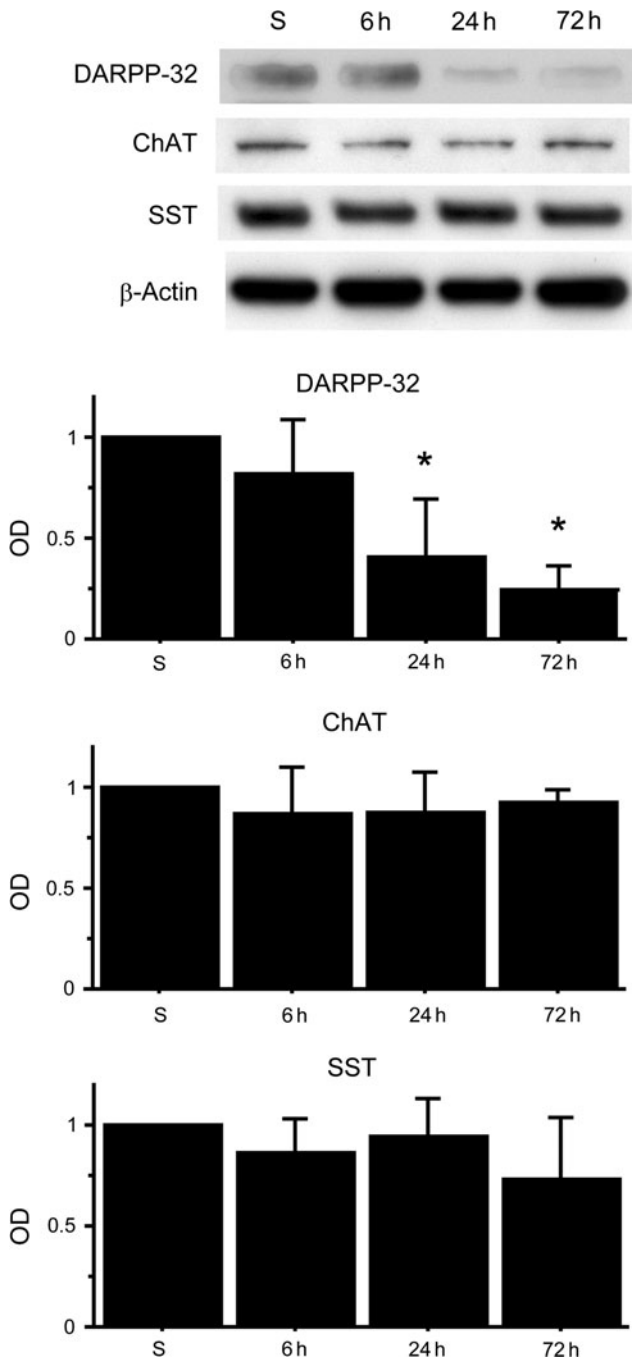

FIG. 6. Western blot analysis of striatal neuronal markers after bilateral common carotid artery occlusion (BCCAO). DARPP-32 expression significantly decreased 24–72 h after BCCAO compared with sham animals ($n = 4$; $^*p < 0.01$). There were no significant changes at any time point in ChAT and SST expression. β-Actin is shown as an internal control (S, sham control; OD, optical density; DARPP-32, anti-dopamine and cyclic AMP-regulated phosphoprotein of relative molecular weight 32,000; ChAT, anti-choline acetyltransferase; SST, anti-somatostatin).

brain region. Although striatal injury after tGCI has not received much attention, some authors have also reported that striatal neurons are the most vulnerable in C57BL/6 mouse brains after tGCI (Gillingwater et al., 2004; Olsson et al., 2003; Terashima et al., 1998; Yang et al., 1997; Yoshioka et al., 2010). Therefore, a striatal injury model that uses C57BL/6 mice can be appropriate for studying neuronal death after tGCI. Although the dorsolateral striatum has been reported to be particularly susceptible to tGCI in rats (Pulsinelli et al., 1982) and gerbils (Crain et al., 1988), there were no significant differences in ischemic vulnerability among the subregions of the striatum in this study. Since Terashima and associates (1998) reported a result similar to ours in C57BL/6 mice, this discrepancy might be explained by the difference in species.

Our exclusion/inclusion criterion of the ischemic animals was based on cortical blood flow measured by LDF. Cortical blood flow during ischemia is well correlated with the patency of the PcomA during ischemic surgery (Kitagawa et al., 1998; Olsson et al., 2003), which was also confirmed in this study. In animals that lack the PcomA, collateral blood flow from the posterior to the anterior circulation is absent, and the forebrains would be ischemic after BCCAO. Ischemic neuronal injury of the hippocampal CA1 subregion, which is not a direct target of LDF measurement, was reported to be induced in mice (Olsson et al., 2003; Yang et al., 1997), rats (Dirnagl et al., 1993), and gerbils (Kuroiwa et al., 1990), when cortical blood flow decreased below 5–15% of the control level. Similarly to these results, we observed consistent injury in deeply located areas such as the striatum and white matter when cortical blood flow decreased. Therefore, even though our exclusion/inclusion criterion was based on cortical blood flow, which was not the focus of the study, we believe that LDF would be very useful for excluding mice that are not ischemic in the striatum and white matter after BCCAO.

We distinguished the subpopulations of striatal neurons by immunohistochemical markers, and showed that DARPP-32-positive MSNs were the most vulnerable after tGCI, which was quantitatively confirmed by Western blot analysis. Using neurochemical methods with radioimmunoassay, Uemura and colleagues (1990) reported that the concentration of substance P, which is contained in a subtype of MSNs, was decreased after tGCI, while that of SST was unchanged in the gerbil striatum. In mice, however, differences in vulnerability after tGCI among the striatal neuronal subpopulations have not been studied in detail. In this study, we evaluated the difference in ischemic vulnerability using immunohistochemistry and Western blot analysis. We show that DARPP-32-positive MSNs were more vulnerable than SST-positive GABAergic interneurons and ChAT-positive cholinergic interneurons, which is consistent with the results obtained by Uemura and associates (1990) using gerbils. DARPP-32, a bifunctional signaling molecule that controls serine/threonine kinase and serine/threonine phosphatase activity, is a critical element of dopaminergic neurotransduction, and is highly enriched in the cytosol of MSNs (Bibb et al., 1999; Nishi et al., 1997). Using this marker, we could distinctly detect MSN injury after tGCI.

Oxidative stress has an important role in neuronal injury during reperfusion following ischemia (Niizuma et al., 2010). Our results suggest that susceptibility to oxidative stress could be one of the mechanisms of ischemic vulnerability in striatal neurons. We showed that oxidative protein injury in the striatum was increased after ischemia. In addition, immunohistochemistry revealed that DNA oxidative injury after ischemia was significant in MSNs. These results indicate the susceptibility of the striatum, especially MSNs, to oxidative

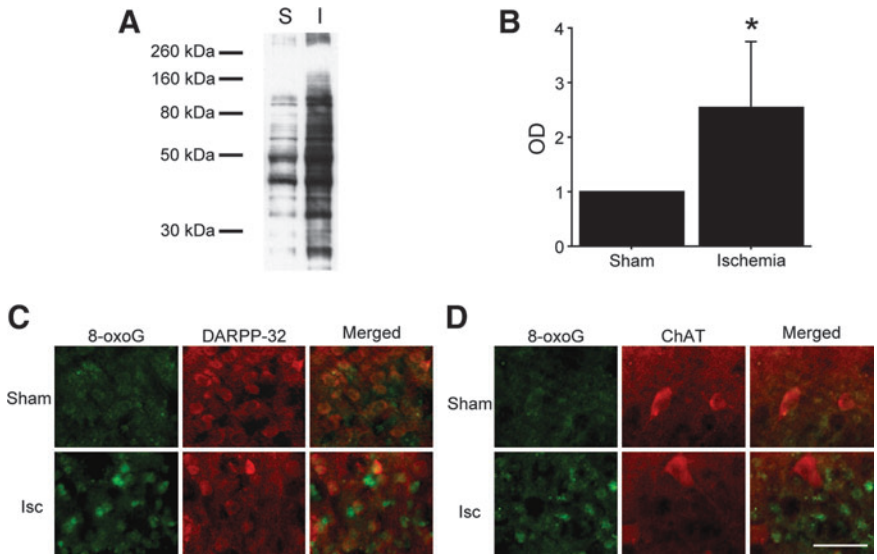

FIG. 7. (**A** and **B**) Quantitative evaluation of oxidative protein damage by detection of the carbonyl groups introduced into proteins. The levels of the carbonyl groups in the striatum significantly increased 24 h after bilateral common carotid artery occlusion (BCCAO) compared with sham animals ($n = 6$; $^*p < 0.05$). (**C** and **D**) Representative photomicrographs of 8-oxoG staining. Expression of 8-oxoG increased in the striatum 24 h after BCCAO. 8-oxoG staining co-localized with DARPP-32 staining; however, it did not co-localize with ChAT staining (magnification × 400; scale bar = 50 μm;. I and Isc, ischemia; 8-oxoG, anti-8-oxoguanine; DARPP-32, anti-dopamine and cyclic AMP-regulated phosphoprotein of relative molecular weight 32,000; ChAT, anti-choline acetyltransferase). Color image is available online at www.liebertpub.com/neu.

injury; however, the mechanism of this susceptibility remains unclear and further studies are needed for clarification.

Although established tGCI models induce consistent hippocampal CA1 injury in rats and gerbils, some authors have reported that consistent CA1 injury is difficult to induce in C57BL/6 mice. First, longer ischemic duration is required in these mice. In previous reports, the required duration of tGCI for C57BL/6 mice has ranged from 10–60 min, and many researchers in recent years have tended to adopt a relatively prolonged ischemic duration such as 20–30 min (Bangsow et al., 2008; Cho et al., 2007; Lee et al., 2008; Walker and Rosenberg, 2009; Zheng et al., 2007). Second, regional vulnerability in the C57BL/6 mouse brain may not be identical to that in rats and gerbils. Namely, some authors reported that the CA2–3 or CA4 subregion was injured, although the CA1 subregion was nearly intact. Moreover, the infrequency of bilateral CA1 injury (25–37.5%) is another problem (Panahian et al., 1996; Yang et al., 1997). All these findings were also observed in the current study. We needed a prolonged duration of ischemia (22 min), and observed non-reproducible injury in the hippocampus. The reason for the differences in ischemic vulnerability of the hippocampus among the rodent species remains unclear. Since the prolonged anoxic depolarization induced by cardiac arrest did not produce CA1 injury in C57BL/6 mice, severe metabolic insult may be required for CA1 injury in these mice (Kawahara et al., 2002; Yonekura et al., 2004). In addition to the metabolic aspect, the infrequency of bilateral CA1 injuries may suggest differences in microcirculation in the hippocampus among rodent species. We will examine blood flow and microcirculation in several brain regions in a future study to clarify the mechanisms involved in this phenomenon.

Protection of white matter is exceedingly important for stroke treatment. About 50% of the adult human brain is composed of cerebral white matter. In addition, white matter is vulnerable to ischemia, since the myelin sheath contains an abundance of lipids, which can be peroxidized after ischemia, and since there are low levels of intrinsic antioxidants in white matter (Ueno et al., 2009). Besides stroke, white matter injury is also observed in patients who suffer transient cardiac arrest. Some authors reported white matter injury after tGCI in rodent models in the stratum radiatum of the CA1 subregion, the cerebral subcortical region, and the corpus callosum (Kubo et al., 2009; Pluta et al., 2006; Walker and Rosenberg, 2010). In the current study, we observed severe white matter injury in the striatum and the cingulum bundle, and mild injury in the external capsule and corpus callosum. The difference in injured regions may be attributable to the differences in ischemic models or evaluation methods. Since the striatum was homogeneously under severe ischemia in the model used in this study, it is reasonable to believe that white matter was injured, as well as neurons. In contrast, we also observed severe injury to the cingulum bundle, which is the structure adjacent to the corpus callosum. The cingulum bundle consists of three major fiber components originating from the thalamus, the cingulum gyrus, and the cortical association areas (Mufson and Pandya, 1984). Since the neuronal injuries in these originating areas were neither severe nor consistent in this study, we conclude that the cingulum bundle is extremely vulnerable to ischemia, although the mechanism remains unclear.

In this study, we detected axonal injury by SMI-32 immunohistochemistry. The SMI-32 antibody reacts with dephosphorylated neurofilament H within the neuronal and axonal cytoskeleton. Neurofilament proteins are highly phosphorylated under physiological conditions, and axonal injury causes a decrease in phosphorylated neurofilament and an

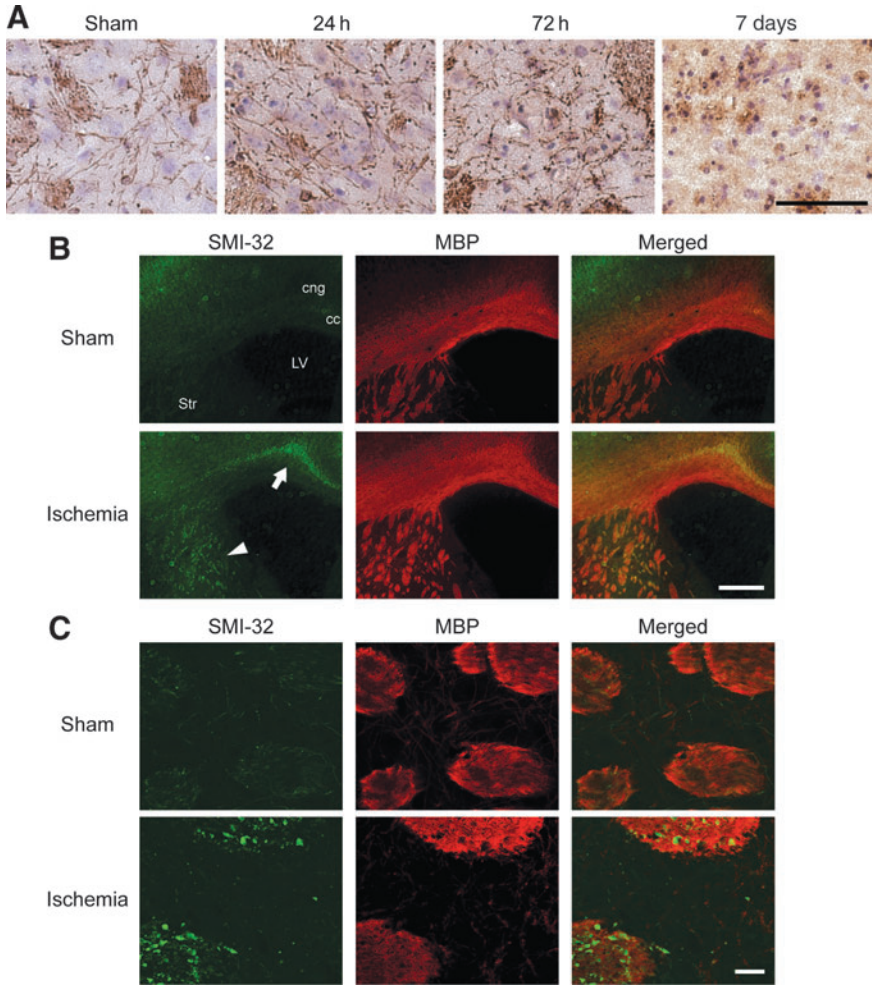

FIG. 8. White matter injury after bilateral common carotid artery occlusion (BCCAO). (**A**) Representative photomicrographs of RIP staining. RIP-positive processes were thin and smooth in the sham animals; however, 72 h after BCCAO they became tangled and intermittent. Seven days after BCCAO, RIP-positive processes disappeared, though the staining of cell bodies was observed. Nuclei were counterstained with hematoxylin (magnification × 400; scale bar = 50 μm). (**B**) Representative low-magnification (× 25) photomicrographs of SMI-32 (green) and MBP (red) staining. Seventy-two hours after BCCAO, intense expression of SMI-32 was observed in the fiber fascicles of the internal capsule of the striatum (arrowhead). The cingulum bundle, large fibers adjacent to the corpus callosum, was also immunopositive for SMI-32 after ischemia (arrow; scale bar = 400 μm). (**C**) Representative high-magnification photomicrographs of SMI-32 (green) and MBP (red) staining of the striatum. Using a confocal microscope, fine neurofilaments and axons among the fiber fascicles were detected in the sham animals. They had disappeared at 72 h after BCCAO. With MBP staining, a coarse change and vacuolation of the fiber fascicles were also observed (scale bar = 20 μm; MBP, anti-myelin basic protein; SMI-32, anti-non-phosphorylated neurofilament; RIP, RNA binding protein immunoprecipitation). Color image is available online at www.liebertpub.com/neu.

increase in dephosphorylated neurofilament (Trapp et al., 1998). Therefore, the SMI-32 antibody can be used to detect axonal injury under many conditions (Gresle et al., 2006). Although many authors have detected axonal injury by amyloid precursor protein immunohistochemistry, assessment of axonal injury with an amyloid precursor protein antibody is limited, because the immunostaining is restricted mainly to the margins of the ischemic lesion, and hence is largely absent from the ischemic core (Gresle et al., 2006; Yam et al., 1997). Therefore, we used SMI-32 immunohistochemistry, and clearly detected axonal injury. To our knowledge, the current study is the first to detect axonal injury after tGCI using SMI-32 immunohistochemistry, and we propose that SMI-32 immunohistochemistry is very sensitive for detection of axonal injury after tGCI.

One limitation of our study with regard to white matter injury is the difficulty of quantitative evaluation. White matter injury was evaluated only by immunostaining, which is difficult to quantify. Some authors have evaluated white matter injury after focal ischemia using an amyloid precursor protein immunoreactivity score (Imai et al., 2001; Yam et al., 1997); however, such scoring systems are not quantitative. We need to develop a quantitative evaluating method in a future study.

In conclusion, we suggest a tGCI model that consistently produces neuronal and white matter injury in C57BL/6 mice with the use of a simple technique. Since C57BL/6 mice are commonly used in the production of transgenic and knockout animals, this model can be highly useful for elucidating *in vivo* molecular mechanisms of ischemic injury in neurons and white matter.

Acknowledgments

This work was supported by grants PO1 NS014543, RO1 NS036147, and RO1 NS038653, from the National Institutes of Health (NIH), and by the James R. Doty Endowment. The content is solely the responsibility of the authors and does not necessarily represent the official views of the NIH. We thank Liza Reola and Bernard Calagui for technical assistance, Cheryl Christensen for editorial assistance, and Elizabeth Hoyte for assistance with the figures.

Author Disclosure Statement

No competing financial interests exist.

References

Bangsow, T., Baumann, E., Bangsow, C., Jaeger, M.H., Pelzer, B., Gruhn, P., Wolf, S., von Melchner, H., and Stanimirovic, D.B. (2008). The epithelial membrane protein 1 is a novel tight junction protein of the blood-brain barrier. J. Cereb. Blood Flow Metab. 28, 1249–1260.

Bibb, J.A., Snyder, G.L., Nishi, A., Yan, Z., Meijer, L., Fienberg, A.A., Tsai, L.H., Kwon, Y.T., Girault, J.A., Czernik, A.J., Huganir, R.L., Hemmings, H.C., Nairn, A.C., and Greengard, P. (1999). Phosphorylation of DARPP-32 by Cdk5 modulates dopamine signalling in neurons. Nature 402, 669–671.

Cho, K.-O., Kim, S.-K., Cho, Y.-J., Sung, K.-W., and Kim, S.Y. (2007). Regional differences in the neuroprotective effect of minocycline in a mouse model of global forebrain ischemia. Life Sci. 80, 2030–2035.

Conlon, K.A., Zharkov, D.O., and Berrios, M. (2003). Immunofluorescent localization of the murine 8-oxoguanine DNA glycosylase (mOGG1) in cells growing under normal and nutrient deprivation conditions. DNA Repair 2, 1337–1352.

Crain, B.J., Westerkam, W.D., Harrison, A.H., and Nadler, J.V. (1988). Selective neuronal death after transient forebrain ischemia in the Mongolian gerbil: a silver impregnation study. Neuroscience 27, 387–402.

Dirnagl, U., Thorén, P., Villringer, A., Sixt, G., Them, A., and Einhäupl, K.M. (1993). Global forebrain ischaemia in the rat: controlled reduction of cerebral blood flow by hypobaric hypotension and two-vessel occlusion. Neurol. Res. 15, 128–130.

Fujii, M., Hara, H., Meng, W., Vonsattel, J.P., Huang, Z., and Moskowitz, M.A. (1997). Strain-related differences in susceptibility to transient forebrain ischemia in SV-129 and C57black/6 mice. Stroke 28, 1805–1810.

Fujimura, M., Morita-Fujimura, Y., Murakami, K., Kawase, M., and Chan, P.H. (1998). Cytosolic redistribution of cytochrome c after transient focal cerebral ischemia in rats. J. Cereb. Blood Flow Metab. 18, 1239–1247.

Gillingwater, T.H., Haley, J.E., Ribchester, R.R., and Horsburgh, K. (2004). Neuroprotection after transient global cerebral ischemia in Wld(s) mutant mice. J. Cereb. Blood Flow Metab. 24, 62–66.

Gresle, M.M., Jarrott, B., Jones, N.M., and Callaway, J.K. (2006). Injury to axons and oligodendrocytes following endothelin-1-induced middle cerebral artery occlusion in conscious rats. Brain Res. 1110, 13–22.

Hwang, I.K., Lee, H.Y., Yoo, K.-Y., Kim, J.C., Kim, J.H., Kim, C.H., Kang, T.-C., Kim, J.D., and Won, M.H. (2006). Rip immunoreactivity significantly decreases in the stratum oriens of hippocampal CA1 region after transient forebrain ischemia in gerbils. Brain Res. 1073–1074, 491–496.

Imai, H., Masayasu, H., Dewar, D., Graham, D.I., and Macrae, I.M. (2001). Ebselen protects both gray and white matter in a rodent model of focal cerebral ischemia. Stroke 32, 2149–2154.

Kamada, H., Yu, F., Nito, C., and Chan, P.H. (2007). Influence of hyperglycemia on oxidative stress and matrix metalloproteinase-9 activation after focal cerebral ischemia/reperfusion in rats. Relation to blood-brain barrier dysfunction. Stroke 38, 1044–1049.

Kawahara, N., Kawai, K., Toyoda, T., Nakatomi, H., Furuya, K., and Kirino, T. (2002). Cardiac arrest cerebral ischemia model in mice failed to cause delayed neuronal death in the hippocampus. Neurosci. Lett. 322, 91–94.

Keskintepe, L., Norris, K., Pacholczyk, G., Dederscheck, S.M., and Eroglu, A. (2007). Derivation and comparison of C57BL/6 embryonic stem cells to a widely used 129 embryonic stem cell line. Transgenic Res. 16, 751–758.

Kirino, T. (1982). Delayed neuronal death in the gerbil hippocampus following ischemia. Brain Res. 239, 57–69.

Kitagawa, K., Matsumoto, M., Tsujimoto, Y., Ohtsuki, T., Kuwabara, K., Matsushita, K., Yang, G., Tanabe, H., Martinou, J.-C., Hori, M., and Yanagihara, T. (1998). Amelioration of hippocampal neuronal damage after global ischemia by neuronal overexpression of BCL-2 in transgenic mice. Stroke 29, 2616–2621.

Kreitzer, A.C. (2009). Physiology and pharmacology of striatal neurons. Annu. Rev. Neurosci. 32, 127–147.

Kubo, K., Nakao, S., Jomura, S., Sakamoto, S., Miyamoto, E., Xu, Y., Tomimoto, H., Inada, T., and Shingu, K. (2009). Edaravone, a free radical scavenger, mitigates both gray and white matter damages after global cerebral ischemia in rats. Brain Res. 1279, 139–146.

Kuroiwa, T., Bonnekoh, P., and Hossmann, K.-A. (1990). Prevention of postischemic hyperthermia prevents ischemic injury of CA_1 neurons in gerbils. J. Cereb. Blood Flow Metab. 10, 550–556.

Lee, K.-J., Jang, Y.-H., Lee, H., Yoo, H.-S., and Lee, S.-R. (2008). PPARγ agonist pioglitazone rescues neuronal cell damage after transient global cerebral ischemia through matrix metalloproteinase inhibition. Eur. J. Neurosci. 27, 334–342.

Mufson, E.J., and Pandya, D.N. (1984). Some observations on the course and composition of the cingulum bundle in the rhesus monkey. J. Comp. Neurol. 225, 31–43.

Murakami, K., Kondo, T., Kawase, M., and Chan, P.H. (1998). The development of a new mouse model of global ischemia: focus on the relationships between ischemia duration, anesthesia, cerebral vasculature, and neuronal injury following global ischemia in mice. Brain Res. 780, 304–310.

Niizuma, K., Yoshioka, H., Chen, H., Kim, G.S., Jung, J.E., Katsu, M., Okami, N., and Chan, P.H. (2010). Mitochondrial and apoptotic neuronal death signaling pathways in cerebral ischemia. Biochim. Biophys. Acta. 1802, 92–99.

Nishi, A., Snyder, G.L., and Greengard, P. (1997). Bidirectional regulation of DARPP-32 phosphorylation by dopamine. J. Neurosci. 17, 8147–8155.

Olsson, T., Wieloch, T., and Smith, M.-L. (2003). Brain damage in a mouse model of global cerebral ischemia. Effect of NMDA receptor blockade. Brain Res. 982, 260–269.

Panahian, N., Yoshida, T., Huang, P.L., Hedley-Whyte, E.T., Dalkara, T., Fishman, M.C., and Moskowitz, M.A. (1996). Attenuated hippocampal damage after global cerebral ischemia in mice mutant in neuronal nitric oxide synthase. Neuroscience 72, 343–354.

Pluta, R., Ułamek, M., and Januszewski, S. (2006). Micro-blood-brain barrier openings and cytotoxic fragments of amyloid

precursor protein accumulation in white matter after ischemic brain injury in long-lived rats. Acta Neurochir. Suppl. 96, 267–271.

Pulsinelli, W.A., Brierley, J.B., and Plum, F. (1982). Temporal profile of neuronal damage in a model of transient forebrain ischemia. Ann. Neurol. 11, 491–498.

Sheng, H., Laskowitz, D.T., Pearlstein, R.D., and Warner, D.S. (1999). Characterization of a recovery global cerebral ischemia model in the mouse. J. Neurosci. Methods 88, 103–109.

Terashima, T., Namura, S., Hoshimaru, M., Uemura, Y., Kikuchi, H., and Hashimoto, N. (1998). Consistent injury in the striatum of C57BL/6 mice after transient bilateral common carotid artery occlusion. Neurosurgery 43, 900–907.

Trapp, B.D., Peterson, J., Ransohoff, R.M., Rudick, R., Mörk, S., and Bö, L. (1998). Axonal transection in the lesions of multiple sclerosis. N. Engl. J. Med. 338, 278–285.

Uemura, Y., Kowall, N.W., and Beal, M.F. (1990). Selective sparing of NADPH-diaphorase-somatostatin-neuropeptide Y neurons in ischemic gerbil striatum. Ann. Neurol. 27, 620–625.

Ueno, Y., Zhang, N., Miyamoto, N., Tanaka, R., Hattori, N., and Urabe, T. (2009). Edaravone attenuates white matter lesions through endothelial protection in a rat chronic hypoperfusion model. Neuroscience 162, 317–327.

Walker, E.J., and Rosenberg, G.A. (2010). Divergent role for MMP-2 in myelin breakdown and oligodendrocyte death following transient global ischemia. J. Neurosci. Res. 88, 764–773.

Walker, E.J., and Rosenberg, G.A. (2009). TIMP-3 and MMP-3 contribute to delayed inflammation and hippocampal neuronal death following global ischemia. Exp. Neurol. 216, 122–131.

Wellons, J.C. III, Sheng, H., Laskowitz, D.T., Mackensen, G.B., Pearlstein, R.D., and Warner, D.S. (2000). A comparison of strain-related susceptibility in two murine recovery models of global cerebral ischemia. Brain Res. 868, 14–21.

Wu, O., Sorensen, A.G., Benner, T., Singhal, A.B., Furie, K.L., and Greer, D.M. (2009). Comatose patients with cardiac arrest: predicting clinical outcome with diffusion-weighted MR imaging. Radiology 252, 173–181.

Yam, P.S., Takasago, T., Dewar, D., Graham, D.I., and McCulloch, J. (1997). Amyloid precursor protein accumulates in white matter at the margin of a focal ischaemic lesion. Brain Res. 760, 150–157.

Yang, G., Kitagawa, K., Matsushita, K., Mabuchi, T., Yagita, Y., Yanagihara, T., and Matsumoto, M. (1997). C57BL/6 strain is most susceptible to cerebral ischemia following bilateral common carotid occlusion among seven mouse strains: selective neuronal death in the murine transient forebrain ischemia. Brain Res. 752, 209–218.

Yonekura, I., Kawahara, N., Nakatomi, H., Furuya, K., and Kirino, T. (2004). A model of global cerebral ischemia in C57BL/6 mice. J. Cereb. Blood Flow Metab. 24, 151–158.

Yoshioka, H., Niizuma, K., Katsu, M., Okami, N., Sakata, H., Kim, G.S., Narasimhan, P., and Chan, P.H. (2010). NADPH oxidase mediates striatal neuronal injury after transient global cerebral ischemia. J. Cereb. Blood Flow Metab. [Epub ahead of print; doi, 10.1038/jcbfm.2010.166].

Zheng, Y.-Q., Liu, J.-X., Wang, J.-N., and Xu, L. (2007). Effects of crocin on reperfusion-induced oxidative/nitrative injury to cerebral microvessels after global cerebral ischemia. Brain Res. 1138, 86–94.

Address correspondence to:
Pak H. Chan, Ph.D.
Neurosurgical Laboratories
Stanford University
1201 Welch Road, MSLS #P314
Stanford, CA 94305-5487

E-mail: phchan@stanford.edu